CIRP Annals - Manufacturing Technology 00 (2025) 1–5

Contents lists available at ScienceDirect

CIRP Annals - Manufacturing Technology

journal homepage: https://www.editorialmanager.com/CIRP/default.aspx

Finding hidden spindle bearing defect periods using Ramanujan filter banks

Mohit Law (2)

Machine Tool Dynamics Laboratory, Department of Mechanical Engineering, Indian Institute of Technology, Kanpur, Uttar Pradesh, India

ARTICLE INFO

Article history:
Available online xxx

Keywords:
Spindle
Monitoring
Defect

ABSTRACT

Classifying defects is difficult when spindle bearings have multiple faults that interact with each other and result in the measured vibrations exhibiting cyclo- and non-stationarity. For such cases, this paper shows that the Ramanujan sum when used as a basis to construct filter banks helps decompose the signal into its individual components that makes it possible to estimate hidden defect periods. Illustrative examples with different spindle types show how filter banks can identify periods not obvious in the signal's Fourier spectra, or in spectrograms, or even those left unclassified by the envelope spectrum method or the empirical mode decomposition method.

1. Introduction

Machine performance is governed by the condition of its spindle and the spindle's bearings [1]. The health of the bearings is influenced by geometrical imperfections resulting from their manufacture, by imbalances and cutting loads, by lubrication and preload settings, and by thermal instabilities. Problems caused by any of these manifest as defects in the bearing's races, in its rolling elements, and/or in its cage. Often, one defect causes others [2,3]. Hence, if defects can be classified correctly, the severity of damage can be assessed to plan repair and avoid breakdown. Defect-driven diagnosis however is not trivial [3,4], especially so when harmonics of multiple different defects interact with each other.

As bearings with defects rotate, different defects cause different periodic impulses. The usual method to hence diagnose defects is to monitor vibrations measured from a sensor placed on the spindle housing. Typical signals of bearings with faults are shown in Fig. 1. If only race defects are present, the signals typically exhibit stationarity, i.e., periods remain constant, and defects can be classified by a simple search for their corresponding frequencies from within the Fourier spectrum [5]. When a cage or ball defect interacts with a race defect, the signal appears to have a carrier frequency corresponding to the race defect that is modulated by the cage or ball defect frequency. Such cyclostationary signals appear to 'beat' with a hidden cyclic frequency and signal structure [2,6]. In such cases, the envelope spectrum method that demodulates the original signal using a Hilbert transform can be used to identify fault frequencies [2,7]. However, even this method fares badly when multiple defects interact with each other and result in a localized change in periods. In such cases when the signal exhibits changing, quasi, and irregular periodicity, i.e., the signal exhibits non-stationarity [2,8], the wavelet transform-based decomposition method [9] or the empirical mode decomposition method [10] can be used. However, since bearings with multiple faults behave like highly nonlinear systems [8], the decomposition methods also sometimes fare poorly.

Since traditional methods of defect-driven diagnosis have their limitations, there is a need for a reliable method for when there are multiple potential defects in the bearings. To address this need, this paper leverages properties of the Ramanujan sum [11] for extracting hidden periodicities in signals. By using the sum as a basis to construct a representation of a measurement, buried periods in the signal can be uncovered [12,13].

Because the use of the sum allows for finding buried periods, the sum was combined in interesting ways with the Fourier series in [14] and with the mode decomposition method in [15,16] to find bearing defects. Though single defects were classified correctly, previous research did not use Ramanujan's ideas to their full potential to identify multiple defects, and nor were the ideas leveraged to track periods changing within measured windows.

Since the sum can also be used as a basis to construct filter banks that separates composite signals into its individual periods [17], a filter bank can localize how periodic components change within measured windows. Hence, the main aim and new contribution of this paper is to demonstrate the use of the sum in filter banks to offer a robust alterative to identify multiple hidden bearing defect periods from signals that exhibit cyclo- and non-stationarity.

Details on how the problem is setup is discussed in Section 2. Simulated examples are discussed in Section 3 to illustrate the workings of the method. Section 4 discuss how the method works with two representative examples of measurements on two different spindle types. In each case, results obtained with filter banks are benchmarked with four other traditional defect classification methods. Conclusions follow in Section 5.

E-mail address: mlaw@iitk.ac.in

https://doi.org/10.1016/j.cirp.2025.04.072

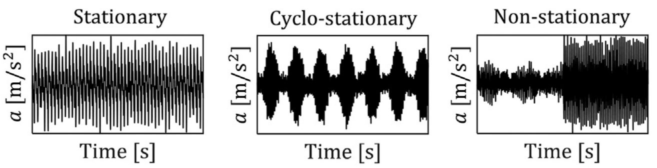

Fig. 1. Typical signals from local faults in rolling element bearings.

2. Period estimation from Ramanujan filter banks

Consider that a discrete time measured vibration signal $a(n)$ of length N can be represented by the Ramanujan sum, $c_q(n)$ as [12]:

$$a(n) = \sum_{q=1}^{N} b_q \underbrace{\sum_{\substack{k=1 \\ (k,q)=1}}^{q} e^{j2\pi kn/q}}_{c_q(n)} \tag{1}$$

wherein n represents integer time, b_q are coefficients, and (k,q) denotes the greatest common divisor. The sum hence runs over those k that are coprime to period q. This representation is sparse since it excludes redundant basis as used in the Fourier transform.

Using the sum as a basis, the periodic components of $a(n)$ can be represented using a Ramanujan dictionary $\mathbf{A}$, columns of which are subspaces made up of the sum [12,13]:

$$\mathbf{a} = \mathbf{A}_{N\times\phi(P_{\max})}\mathbf{y} \tag{2}$$

wherein $\mathbf{a} = [\,a(0) \quad a(1) \quad \ldots \quad a(N-1)\,]^T$, $P_{\max}$ is the maximum period to be found and $\phi(P_{\max})$ means the number of integers in $[1, P_{\max}]$ coprime to $P_{\max}$. Since $\mathbf{a}$ and $\mathbf{A}$ are known, $\mathbf{y}$, which contains the hidden periods in $\mathbf{a}$ is to be found.

To find $\mathbf{y}$, and to track localized changes in periods in signals exhibiting cyclo- and non-stationarity, Ramanujan filter banks can be used [17]. The filter bank contains frequency responses:

$$C_q\left(e^{j\omega}\right) = \mathscr{F}[c_q(n)],\ 1 \le q \le P_{\max} \tag{3}$$

wherein $\mathscr{F}[\cdot]$ is the Fourier transform of the qth Ramanujan sum. Since $c_q(n)$ is periodic, the line spectrum of $C_q(e^{j\omega})$ is nonzero only at $(2\pi k_i/q)$ where k_i is coprime to q. Thus, a valid estimation of the multiple hidden periods $\{p_i\}$ in $a(n)$ is possible by considering the least common multiple of all filter indices [12].

Due to $a(n)$ having a finite length N, the filters can be represented as finite impulse response filters [12,17]:

$$C_q^{(l)}(z) = \sum_{n=0}^{ql-1} c_q(n) z^{-n} \tag{4}$$

wherein each filter $c_q^{(l)}(n)$ is truncated to l periods. Since the duration of the qth filter is ql samples, localization of periods is extractable such that if $a(n)$ has different periodic components localized at different times, then by examining the filter bank output as a function of time, i.e., by looking at a plot of $y_P(n)$ for different periods P across different n results in a time-period plane plot that contains the localization information.

3. Illustrating filter banks with simulated examples

Period estimation capabilities of filter banks are illustrated with simulated signals exhibiting stationarity, cyclostationarity, and non-stationarity. One second duration signals were generated in MATLAB by sampling at frequencies of $f_{ss} = 8192$ Hz, i.e., $N = 8192$. The double subscript ‘s’ represents simulations. Fig. 2 shows shorter durations of these signals to reveal their characteristics. Gaussian white noise was added to signals such that the signal to noise ratio (SNR) was 10. The stationary signal was assumed to be a sum of two periods: one period 27 signal corresponding to a spindle rotational frequency of $f_{SP_s} = 300$ Hz, and another period 3 signal corresponding to an outer race defect frequency of $f_{O_s} = 2731$ Hz. In addition to these two periods, the cyclostationary signal was also synthesized to contain a period 67 signal corresponding to a cage defect frequency of $f_{C_s} = 123$ Hz that modulates f_{O_s}. The non-stationary signal is like the cyclostationary one, except for the later 0.5 s, which has two additional periods: one period 14 signal corresponding to a rolling element defect frequency of $f_{B_s} = 585$ Hz that modulates a period corresponding to an inner race defect frequency of $f_{I_s} = 3095$ Hz. Periods in all cases are the ratios of the sampling frequency, f_{ss} to defect frequencies ($f_{O_s}, f_{I_s}, f_{B_s}, f_{C_s}$).

Results with filter banks are benchmarked with those obtained from a Fourier transform, with the short-time Fourier transform (STFT), the envelope spectrum [7] and the empirical mode decomposition (EMD) method [10] – as shown in Fig. 2. Filter bank outputs were normalized between 0 and 1, and then thresholded to zero for values < 0.1 such as to only retain strong periods.

For the stationary signal type, all but the EMD method, correctly classify periods (frequencies) corresponding to f_{O_s} and f_{SP_s}. Since the periods do not change in a stationary signal, this is expected, and the use of filter banks in this case offers no real advantage. For the EMD method, the spectrum of the first intrinsic mode function (IMF) shown in Fig. 2(e) has too wide a spread due to noise. The EMD was found to correctly classify defects for a SNR of 100.

The Fourier spectrum in Fig. 2(b) of the cyclostationary signal shows the carrier frequency corresponding to f_{O_s} to be flanked by side bands corresponding to f_{C_s}. The STFT in Fig. 2(c) also shows these side bands, but they are localized and weaker. The spectrum of the envelope shown in Fig. 2(d) has one dominant peak corresponding to a harmonic of f_{C_s}. The EMD method fares poorly in this case too. The output of the filter banks in Fig. 2(f) shows the two fundamental periods corresponding to f_{O_s} and f_{C_s}.

For the signal exhibiting non-stationarity, only the filter banks can identify how the periods change across time. In addition to the two fundamental periods corresponding to f_{O_s} and f_{C_s}, the filter banks

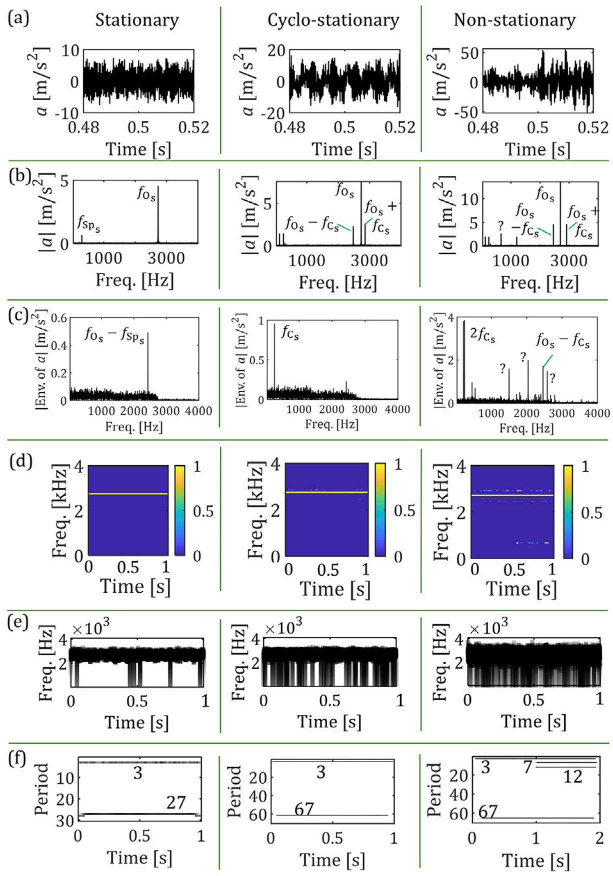

Fig. 2. (a) Three types of synthetic signals, (b) Fourier spectra, (c) Spectra of the envelope (d) Spectrograms normalized between 0 and 1, (e) Hilbert spectra of the 1st IMF, (f) Time-period plots obtained using filter banks.

also identify a period 7 signal that corresponds to the first harmonic of the f_{Bs}, and a period 12 signal corresponding to an interaction of f_{Is} and a harmonic of f_{Bs}. All other methods fail to correctly classify these two defects and their interactions which appear only in the later 0.5 s on the signal.

These simulated examples illustrate the advantages of filter banks in classifying fundamental defect periods in signals exhibiting cyclostationarity, and in uncovering hidden quasi, and irregular periodicities buried with other defect periods in signals exhibiting non-stationarity. Since measured vibration signals with multiple potential defects will also likely exhibit cyclo and non-stationarity, use of filter banks is expected to offer robust defect classification capabilities − as is discussed in Section 4.

4. Finding bearing defects from measured spindle vibrations

Two different high-speed spindle types, one with a motor coupled to the spindle shaft, and another electro-spindle, were measured following protocols in [18,19]. Both spindles had the same bearings mounted in pairs. For confidentiality reasons, details about mounting configurations, sizes, make, and lubrication and cooling conditions of the spindle bearings cannot be revealed. Accelerometers were placed near the front and rear bearing locations and balanced tool holders were used. Spindles were run at different speeds and data was acquired using a PRUFTECHNIK-make hand-held device. Data was sampled at f_s of 32,768 Hz for two seconds, i.e., N was 65,536. All measurements were repeated, and uncertainty was observed to within the acceptable limit of ± 10% [18,19]. Fig. 3 exemplifies the measuring system.

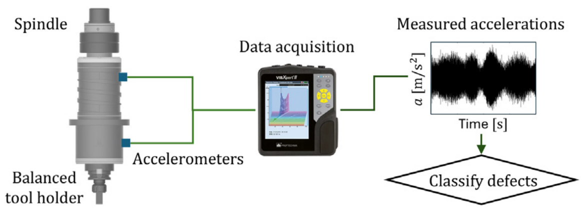

Fig. 3. An illustration of the measurement system.

Though both spindles were on machines that were producing parts with required quality, measurements made as part of a routine condition monitoring exercise raised some concerns about the spindle's health. Diagnosis of potential defects was hence necessary. All defect-driven diagnosis presented herein is for a representative spindle rotation frequency of $f_{SP} = 300$ Hz. Bearing defect frequencies were evaluated using relationships that assume no slip, and relate defect frequencies to bearing geometry, contact angle, number of balls, and the rotational speed [2]. For the speed of interest, race defect frequencies were evaluated to be $f_O = 3124.5$ Hz for the outer race, and $f_I = 3775.5$ Hz for the inner race. Ball defect frequency was evaluated to be $f_B = 1428.1$ Hz, and the cage defect frequency was evaluated to be $f_C = 135.8$ Hz. These frequencies are to be classified if defects are present.

Measurements were low pass filtered with a cut-off frequency of 10 kHz to ensure that harmonics of defects were not filtered out. For analysis with the filter banks, the threshold was set to 0.1, and P_{max} was set to 250, i.e., to be more than the period corresponding to the lowest known defect frequency ($f_s/f_C \cong 242$). Results were benchmarked with other methods as in Section 3.

4.1. Analysis for the directly coupled spindle

Measured vibrations for the directly coupled spindle are shown in Fig. 4(a). For the first half, the response exhibits a 'beating' type cyclostationary behavior typical of one defect frequency being modulating by another. In the second half of the measurement, the response appears to increase approximately linearly. Since nothing in the operational condition has changed during the measurement, the change in the response suggests there are a series of high energy pulses that

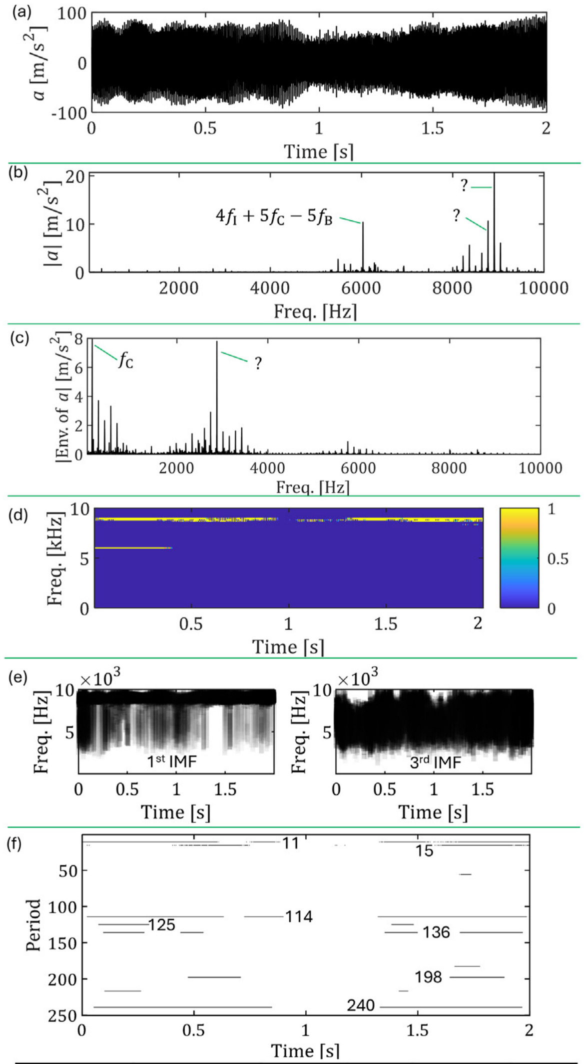

Period	11	15	114	198	240
Freq. [Hz]	2979	2341	287	165	137
Defect	$2f_B + f_C$	$f_I - f_B$	$2f_C$	$f_{Sp} - f_C$	f_C

Fig. 4. (a) Measured vibrations on a coupled spindle, (b) Fourier spectrum, (c) Spectrum of the envelope, (d) Spectrogram normalized between 0 and 1, (e) Hilbert spectra for two IMFs (1st and 3rd), (f) Time-period plot obtained using filter banks along with periods, frequencies, and defects.

result from multiple moving and/or stationary bearing defects interacting with each other as the spindle rotates. This may in turn result in a change of periods within the signal that makes the signal exhibit non-stationarity.

Since the Fourier spectrum in Fig. 4(b) is an average of the magnitude of the different components over the time window, it fails to classify how/if the periods change. Moreover, though the spectrum has several peaks, only the 6031 Hz is correctly identified as corresponding to higher order harmonics of f_I interacting with f_B and f_C. Though harmonic interactions up to the fifth order were tracked, the peaks at 8911 Hz and at 8775 Hz could not be classified correctly. The difference between these is f_C, i.e., the signal is modulated by f_C as is evident from the spectrum of the envelope in Fig. 4(c) which shows peaks at f_C and its harmonics. The other dominant peak at 2879 Hz that has side bands at $\pm f_C$ cannot be classified, likely due to the spectrum of the envelope also not accounting for how the signal changes. However, even the STFT shown in Fig. 4(d) does not reveal fundamental defect frequencies. These results were with a window size of 256. Changing the window did not improve results. The EMD method too performs poorly. Hilbert spectrums of the 1st and 3rd IMFs have too wide a spread and nothing is clearly identifiable.

Results with the Ramanujan filter banks in Fig. 4(f) clearly show how different periods appear to dominate the response at different

Please cite this article as: M. Law, Finding hidden spindle bearing defect periods using Ramanujan filter banks, CIRP Annals - Manufacturing Technology (2025), https://doi.org/10.1016/j.cirp.2025.04.072

times within the measured window. Periods 114 and 240 that correspond to cage defects are present in most of the measured window. Period 11 appears to be stronger at the start of the measurement and corresponds to an interaction between defective balls and defects in the cage. Period 15 becomes stronger during the later part and corresponds to a fundamental interaction of defects in the ball and the inner race. Period 198 which is also stronger during the later part corresponds to a fundamental modulated interaction of the rotational speed with a cage defect. Periods 125 and 136 are weaker and are active for short durations. The use of the filter banks with this example illustrates how the method can help find hidden spindle defect periods and track how these change in signals exhibiting cyclo- and non-stationarity.

4.2. Analysis for the electro-spindle

Measured vibrations for this spindle type shown in Fig. 5(a) also exhibit cyclostationarity. Though the nature of 'beating' in this case is different than that observed in Fig. 4(a), it is again likely that there is a modulated interaction of two or more defects. This is evident from the Fourier spectrum in Fig. 5(b) that shows peaks at 5060 Hz, 8326 Hz, and at 8871 Hz that correspond to harmonics of multiple bearing defects interacting with each other. The modulations are further confirmed from the spectrum of the envelope shown in Fig. 5(c) that shows dominant peaks at the cage defect frequency f_C and its harmonics, as well as a peak corresponding to the fundamental ball defect frequency f_B. There is also a peak at 3409 Hz corresponding to higher order interactions between the ball and cage defects. Though the combined use of the Fourier spectrum and the envelope spectrum can classify all bearing defects (this was also shown possible with the simulated example), how/if these defect periods change in the measured window is not clear. The STFT in Fig. 5(d) and the Hilbert spectra in Fig 5(e) of two representative IMF's from using the EMD also do not help localize how defects change with time.

The time-period plot shown in Fig. 5(f) on the other hand clearly shows how periods change in the measured window. No dominant periods are observed in the initial 0.5 s of the measurement. After which time, there appear to be five dominant periods. Of these, period 240 corresponds to the fundamental cage defect frequency. Periods 48 and 122 correspond to harmonics of f_C. Period 11 corresponds to a frequency of 2979 Hz and is related to a ball defect interacting with a cage defect. Period 4 corresponds to a frequency of 8192 Hz and is related to first order interactions of all four defects. It is worth nothing that even though these period 4 and 11 signal components are divisors of N, these could not be classified with the Fourier spectrum. This example also illustrates how filter banks detect and help track hidden bearing defects.

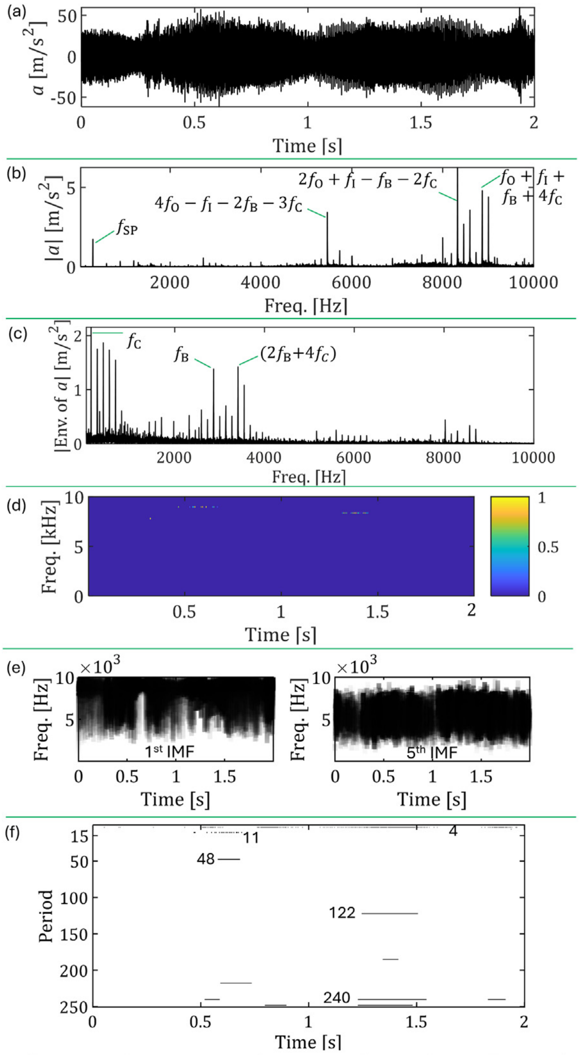

Period	4	11	48	122	240
Freq. [Hz]	8192	2979	683	269	137
Defect	$f_O + f_I + f_B - f_C$	$2f_B + f_C$	$5f_C$	$2f_C$	f_C

Fig. 5. (a) Measured vibrations on an electro-spindle, (b) Fourier spectrum, (c) Spectrum of the envelope (d) Spectrogram normalized between 0 and 1, (e) Hilbert spectra of two IMFs (1st and 5th), (f) Time-period plot obtained using filter banks along with periods, frequencies, and defects.

5. Conclusions

This paper showed that when bearings have multiple defects that interact with each other and make the measured vibrations exhibit cyclo- and non-stationarity, then, the Ramanujan sum when used as a basis to construct filter banks offers a robust alternative to estimating defect periods. The method was illustrated with simulations and measurements on two different spindle types by identifying fundamental bearing defect periods, their interactions, and by tracking how these change in the measured window.

Though only integer periods are identifiable with the use of Ramanujan filter banks, the method still fares better than traditional methods. Even when defect periods were divisors of the length of the signal, the Fourier spectrum and the spectrum of the envelope could not classify them, but the Ramanujan method could. Likewise, the Ramanujan method could classify defects changing in the measured window, which spectrograms and the empirical mode decomposition method failed to do.

Though the workings of Ramanujan sum-based method were illustrated with three simulated and two measured examples, the method was found to be robust in classifying defects in tens of other measurements. Since correctly classifying defects is necessary for defect-driven diagnostics, the method holds promise for spindle health prognostics to predict remaining useful life.

Declaration of competing interest

The authors declare that they have no known competing financial interests or personal relationships that could have appeared to influence the work reported in this paper.

CRediT authorship contribution statement

Mohit Law: Writing – review & editing, Writing – original draft, Visualization, Validation, Supervision, Software, Resources, Project administration, Methodology, Investigation, Funding acquisition, Formal analysis, Data curation, Conceptualization.

Please cite this article as: M. Law, Finding hidden spindle bearing defect periods using Ramanujan filter banks, CIRP Annals - Manufacturing Technology (2025), https://doi.org/10.1016/j.cirp.2025.04.072

References

[1] Abele E, Altintas Y, Brecher C (2010) Machine tool spindle units. *CIRP Annals* 59 (2):781–802.
[2] Randall R B (2011) *Vibration-Based Condition Monitoring: Industrial, Automotive and Aerospace Applications*, John Wiley & Sons Ltd. NJ 07030, USA.
[3] Castelbajac C de, Ritou M, Laporte S, Furet B (2014) Monitoring of distributed defects on HSM spindle bearings. *Applied Acoustics* 77:159–168.
[4] Vogl G W, Donmez M A (2015) A defect-driven diagnostic method for machine tool spindles. *CIRP Annals* 64(1):377–380.
[5] Vafaei S, Rahnejat H, Aini R (2002) Vibration monitoring of high speed spindles using spectral analysis techniques. *International Journal of Machine Tools and Manufacture* 42:1223–1234.
[6] Antoni J (2009) Cyclostationarity by examples. *Mechanical System and Signal Processing* 23:987–1036.
[7] Tai C-Y, Altintas Y (2023) A hybrid physics and data-driven model for spindle fault detection. *CIRP Annals* 72(1):297–300.
[8] Chu F, Zhang Z (1997) Periodic, quasi-periodic and chaotic vibrations of a rub-impact rotor system supported on oil film bearings. *International Journal of Engineering Science* 35(10/11):963–973.
[9] Kankar P K, Sharma S, Harsha S (2011) Fault diagnosis of ball bearings using continuous wavelet transform. *Applied Soft Computing* 11(2):2300–2312.
[10] Huang N E, Shen Z, Long S R, Wu M C, Shih H H, Zheng Q, Yen N-C, Tung C C, Liu H H (1998) The empirical mode decomposition and the Hilbert spectrum for nonlinear and non-stationary time series analysis. *Proceedings of the Royal Society A: Mathematical, Physical and Engineering Sciences* 454:903–995.
[11] Ramanujan S (1918) On certain trigonometrical sums and their applications in the theory of numbers. *Transactions of the Cambridge Philosophical Society* XXII:259–276.
[12] Vaidyanathan P P, Tenneti S (2019) Srinivasa Ramanujan and signal-processing problems. *Proceedings of the Royal Society A: Mathematical, Physical and Engineering Sciences* 378:20180446.
[13] Tenneti S, Vaidyanathan P P (2015) Nested periodic matrices and dictionaries: new signal representations for period estimation. *IEEE Transactions on Signal Processing* 63:3776–3790.
[14] Cheng J, Pan H, Zheng J (2024) A novel feature extraction method: iterative Ramanujan Fourier mixture spectrum. *Structural Health Monitoring* 23(6):3299–3311.
[15] Ma C, Yang Z, Xu Y, Hu A, Zhang K (2023) Periodic detection mode decomposition and its application in bearing fault diagnosis. *IEEE Sensors Journal* 23(11):11806–11814.
[16] Cheng J, Yang Y, Xin L, Chang J (2021) Adaptive periodic mode decomposition and its application in rolling bearing fault diagnosis. *Mechanical System and Signal Processing* 161:107943.
[17] Tenneti S, Vaidyanathan P P (2015) Ramanujan filter banks for estimation and tracking of periodicities. *International Conference on Acoustics, Speech and Signal Processing (ICASSP), Australia*.
[18] International Organization for Standardization (2017) *ISO/DTR 17243-2:* Machine tool spindles — Evaluation of machine tool spindle vibrations by measurements on spindle housing — Part 2: Direct driven spindles and belt driven spindles with rolling element bearings operating at speeds between 600 min^{-1} and 30 000 min^{-1}, ISO, Geneva, Switzerland.
[19] International Organization for Standardization (2014) *ISO/TR 17243-1:* Machine Tool Spindles – Evaluation of Spindle Vibrations by Measurements on Non-Rotating Parts – Part 1: Motor Spindles Measured at Speeds between 600 min^{-1} and 30000 min^{-1} *Supplied with Rolling Element Bearings*, ISO, Geneva, Switzerland.

Please cite this article as: M. Law, Finding hidden spindle bearing defect periods using Ramanujan filter banks, CIRP Annals - Manufacturing Technology (2025), https://doi.org/10.1016/j.cirp.2025.04.072